

DESY 93-021
February 1993

ISSN 0418-9833

The weak electroweak phase transition

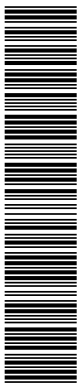
W. Buchmüller, Z. Fodor¹, T. Helbig and D. Walliser²
Deutsches Elektronen-Synchrotron DESY, Hamburg, Germany

Abstract

We present a detailed analysis of the phase transition in the standard model at finite temperature. Using an improved perturbation theory, where plasma masses are determined from a set of one-loop gap equations, we evaluate the effective potential $V_{eff}(\varphi, T)$ in next-to-leading order, i.e., including terms cubic in the gauge coupling g , the scalar self-coupling $\lambda^{1/2}$ and the top-quark Yukawa coupling f_t . The gap equations yield a non-vanishing magnetic plasma mass for the gauge bosons, originating from the non-abelian self-interactions. We discuss in detail size and origin of higher order effects and conclude that the phase transition is weakly first-order up to Higgs masses of about 70 GeV , above which our calculation is no longer self-consistent. For larger Higgs masses even an approximation containing all g^4 contributions to V_{eff} is not sufficient, at least a full calculation to order g^6 is needed. These results turn out to be rather insensitive to the top-quark mass in the range $m_t = 100 - 180 \text{ GeV}$. Using Langer's theory of metastability we calculate the nucleation rate of critical droplets and discuss some aspects of the cosmological electroweak phase transition.

¹Humboldt Fellow, on leave from Institute for Theoretical Physics, Eötvös University, Budapest, Hungary

²Present address: Fermilab, Batavia, IL 60510, USA



1 Introduction

In the standard model the electroweak gauge symmetry is spontaneously broken. However, at sufficiently high temperatures, above a critical temperature of about 100 GeV , the $SU(2) \times U(1)$ symmetry of weak and electromagnetic interactions is restored [1]-[2]. Only many years after the first studies of symmetry restoration it was realized that in the standard model the rates of anomalous baryon- and lepton-number violating processes are unsuppressed at high temperatures [3]. This has important cosmological implications. In particular, it opens the possibility to understand, at least in principle, the generation of the baryon asymmetry of the universe within the standard model. Clearly, the study of "electroweak baryogenesis" requires a detailed knowledge of the transition from the symmetric to the broken phase in the standard model. Recently, this has led to a renewed interest in the electroweak phase transition [4]-[17].

Despite the fact that several important steps towards the understanding of the phase transition have already been made, we are still far from a complete description of this intriguing phenomenon. To a large extent this is due to the infrared problems of perturbative finite-temperature field theory. One manifestation of these infrared problems is the appearance of spurious terms in the effective potential $V_{eff}(\varphi)$, which are linear in the Higgs field φ [7]. On the other hand, it has been argued (cf. [5, 8, 9]) that the effective potential does not have a linear term. A related problem is the contribution of high order loop diagrams to low orders in the coupling constants. This can be understood in terms of dynamically generated plasma masses which damp infrared divergences. Much work has been devoted to the summation of daisy, superdaisy and other types of diagrams which yield higher order corrections to the effective potential [6]-[11]. The free energy has also been evaluated in the $1/N$ -expansion [12] and for background fields averaged over a finite volume [13]. Another important question concerns the decay of a metastable phase via nucleation, growth and coalescence of critical droplets. Furthermore, in the case of a weak first-order transition subcritical droplets and large thermal fluctuations are of importance [17].

In a recent paper [8], the phase transition in scalar electrodynamics was studied in detail. Using an improved perturbation theory, where plasma masses were incorporated from the beginning, the effective potential was calculated to order e^3 and $\lambda^{3/2}$, and it was explicitly demonstrated that the

spurious linear terms cancel. A complete set of one-loop gap equations was evaluated and used to determine a region in the plane of couplings (e^2, λ) where the symmetric phase is metastable. Following the theory of Langer [18] the nucleation rate of critical droplets was calculated, and it was shown that a cosmological phase transition would have been first-order up to Higgs boson masses of the order of the vector boson mass.

In this paper we extend the approach of ref. [8] to the standard model. We study an $SU(2)$ gauge theory, i.e., the case $g' = 0$. This corresponds to the approximation where the W -bosons and the Z -boson are degenerate in mass. We take into account the three generations of fermions, with left-handed doublets and right-handed singlets. The only relevant Yukawa coupling is the top-quark coupling f_t . The effect of the other Yukawa-couplings is negligible.

The outline of the paper is as follows. In sect. 2 we introduce our notation and study one- and two-loop contributions to the finite-temperature effective potential. We then discuss the breakdown of the ordinary perturbative approach and stress the need for an improved perturbation theory. Sect. 3 is devoted to the structure of the vacuum polarisation tensor in spontaneously broken gauge theories at finite temperature. In sect. 4 we evaluate the effective potential. We perform a ring summation, thus collecting all terms of order g^3 and $\lambda^{3/2}$, and we obtain a complete set of one-loop gap equations for the $SU(2)$ gauge theory at finite temperature, which yield a non-vanishing magnetic plasma mass. Using the iterative solution of these gap equations we evaluate the effective potential up to cubic terms in the couplings. The equivalence of this method to the ring summation is shown, and some properties of the potential are studied analytically. Sect. 5 contains a detailed analysis of higher order effects. We study the convergence of the improved perturbation theory, the influence of the obtained transverse plasma mass on the surface tension and the effect of superdaisy diagrams to order g^4 and λ^2 . Following the theory of Langer [18] we compute the nucleation rate of critical droplets in sect. 6, where we also determine the nucleation temperature of a cosmological phase transition. A summary of our results and concluding remarks comprise sect. 7.

Three appendices deal with matters peripheral to the main line of our discussion. In appendix A we prove that the ring summation with self-energy insertions at zero momentum yields all terms of order g^3 and $\lambda^{3/2}$ in the effective potential. Appendix B gives the result of the "superdaisy"-type summation to order g^4 and λ^2 . Appendix C contains some details needed for

the computation of the nucleation rate.

2 Conventional perturbative approach

Let us consider the $SU(2)$ gauge theory described by the Lagrangian \mathcal{L} depending on a set of bosonic and fermionic fields,

$$\mathcal{L} = \mathcal{L}_{gauge} + \mathcal{L}_{Higgs} + \mathcal{L}_{fermion} + \mathcal{L}_{gauge\ fixing} + \mathcal{L}_{ghost}. \quad (1)$$

Using standard conventions the bosonic part reads

$$\begin{aligned} \mathcal{L}_{gauge} + \mathcal{L}_{Higgs} = & -\frac{1}{4}F_{\mu\nu}^a F^{a\mu\nu} + (D_\mu \Phi)^\dagger (D^\mu \Phi) - \mu(\Phi^\dagger \Phi) - \lambda(\Phi^\dagger \Phi)^2, \\ & \mu < 0, \quad D_\mu = \partial_\mu - ig\frac{\tau^a}{2}W_\mu^a, \quad a = 1, 2, 3, \end{aligned} \quad (2)$$

where the Higgs field Φ is an $SU(2)$ doublet. The fermionic part is given by

$$\mathcal{L}_{fermion} = \bar{\psi}_L i\gamma^\mu D_\mu \psi_L + f_t \overline{\begin{pmatrix} t \\ b \end{pmatrix}}_L (i\tau_2 \Phi^*) t_R + h.c. \quad (3)$$

Here τ^a , $a = 1, 2, 3$, denote the Pauli matrices, ψ_L stands for all left-handed fermions and f_t is the Yukawa coupling of the top-quark. All other Yukawa couplings are much smaller and can be neglected. The gauge-fixing and ghost Lagrangians read

$$\mathcal{L}_{gauge\ fixing} = -\frac{1}{2\eta} G_a G^a, \quad G_a = \partial_\mu W_a^\mu - \frac{1}{2}\eta g \varphi \chi_a, \quad (4)$$

$$\mathcal{L}_{ghost} = \bar{c}_a M^{ab} c_b, \quad \delta G^a = M^{ab} \delta \omega_b; \quad (5)$$

here the $SU(2)$ doublet Φ of scalar fields has been written as

$$\Phi = \frac{1}{\sqrt{2}} \begin{pmatrix} \chi_1 + i\chi_2 \\ \varphi + h + i\chi_3 \end{pmatrix}, \quad (6)$$

where h is the Higgs field, χ_a ($a = 1, 2, 3$) are the three Goldstone bosons and φ is a constant background field. In the following we will use Landau gauge, i.e., we take the limit $\eta \rightarrow 0$. The classical minimum is at $\varphi = v \equiv \sqrt{-\mu/\lambda}$.

The tree-level vector boson mass m , the top-quark mass m_t , the Higgs boson mass \bar{m}_φ and the Goldstone boson mass \bar{m}_χ are given by

$$m^2 = \frac{g^2 \varphi^2}{4}, \quad m_t^2 = \frac{f_t^2}{2} \varphi^2, \quad (7)$$

$$\bar{m}_\varphi^2 = \lambda(3\varphi^2 - v^2), \quad \bar{m}_\chi^2 = \lambda(\varphi^2 - v^2). \quad (8)$$

Note that \bar{m}_φ^2 and \bar{m}_χ^2 are negative for small values of φ . The connection between couplings and zero-temperature masses reads $g = 2m_W/v$, $f_t = \sqrt{2}m_t/v$ and $\lambda = m_H^2/2v^2$, where $v = 246 \text{ GeV}$.

The finite temperature action is given by the integral

$$S_\beta = \int_\beta dx \mathcal{L}, \quad (9)$$

with

$$\int_\beta dx \equiv \int_0^\beta d\tau \int d^3x, \quad \beta = \frac{1}{T}. \quad (10)$$

Boson and fermion fields have to satisfy periodic and antiperiodic boundary conditions in τ , respectively.

The finite-temperature effective potential can be perturbatively evaluated in the loop expansion (cf. ref. [19]). The one-loop contribution is shown in fig. 1. Its temperature dependent part can be calculated using standard techniques. The sum of the leading term in the high temperature expansion and the tree-level potential yields:

$$V_0(\varphi) + V_1^{(1)}(\varphi, T) = \frac{1}{2} \left(\frac{3g^2 + 8\lambda + 4f_t}{16} T^2 - \lambda v^2 \right) \varphi^2 + \frac{1}{4} \lambda \varphi^4. \quad (11)$$

As is well known, this potential predicts a second-order phase transition. Note, that the finite-temperature contribution due to scalar loops is proportional to λ and therefore of the same order as the tree-level term $\lambda \varphi^4/4$.

Going one order further in the high-temperature expansion one obtains

$$\begin{aligned} V_0(\varphi) + V_1^{(2)}(\varphi, T) = & \frac{1}{2} \left(\frac{3g^2 + 8\lambda + 4f_t}{16} T^2 - \lambda v^2 \right) \varphi^2 + \frac{1}{4} \lambda \varphi^4 \\ & - \left(9m^3 + \bar{m}_\varphi^3 + 3\bar{m}_\chi^3 \right) \frac{T}{12\pi}. \end{aligned} \quad (12)$$

The potentials (11) and (12) differ in several important respects:

(i) We are faced with the familiar problem that \bar{m}_φ and \bar{m}_χ become imaginary for small values of φ , i.e., the naive one-loop effective potential is complex. This phenomenon is not an artefact of the high-temperature expansion, since the exact one-loop contribution of the Higgs field is proportional to

$$J_+(m_\varphi^2) = \int_0^\infty dx x^2 \log \left(1 - e^{-\sqrt{x^2 + (3\varphi^2 - v^2)\lambda/T^2}} \right), \quad (13)$$

which is also complex for small values of φ . A similar expression is obtained for the Goldstone fields, and no cancellation appears between the two contributions. At zero temperature, the imaginary part of the potential has been related to the lifetime of a particular quantum state [20].

(ii) The new cubic terms are of order g^3 and $\lambda^{3/2}$, and thus of higher order than the finite-temperature corrections in $V_1^{(1)}$. Clearly, these new contributions must be combined with terms of the same order which appear in higher order loop diagrams.

(iii) The cubic terms originate from integrals which are infrared divergent for vanishing masses. No cubic term results from the top-quark loop, since the fermionic modes always have non-zero Matsubara frequencies ($\omega_n = (2n+1)\pi T$), and hence do not suffer from infrared problems.

(iv) In order to see the qualitative features of the effective potential (12) we first ignore the terms proportional to $\lambda^{3/2}$, which can be justified for $\lambda \ll g^2$. For temperatures above a certain "barrier" temperature T_b , the second derivative of this modified potential is positive, thus the symmetric phase is a local minimum of the effective potential. Here the barrier temperature T_b is

$$T_b^2 = \frac{16\lambda v^2}{3g^2 + 8\lambda + 4f_t^2}. \quad (14)$$

In eq. (12) the terms proportional to φ^3 and φ^4 have opposite signs. As a result of a compensation between these two terms, for temperatures close enough to T_b , another minimum exists which, at a critical temperature T_c , is degenerate with the minimum at $\varphi = 0$. Hence, in this approximation the phase transition is first-order.

According to (ii) we have to consider higher loop terms involving boson fields, first the two-loop contributions shown in fig. 2. These graphs yield

linear terms in the temperature dependent part of the effective potential:

$$V_2^{(scalar)}(\varphi, T) = -\frac{1}{128\pi}(3g^2 + 8\lambda + 4f_t^2)(\bar{m}_\varphi + 3\bar{m}_\chi)T^3 + \mathcal{O}(g^4, \lambda^2) \quad , \quad (15)$$

$$V_2^{(vector)}(\varphi, T) = -\frac{11}{32\pi}g^3\varphi T^3 + \mathcal{O}(g^4, \lambda^2) \quad . \quad (16)$$

The expressions are cubic in the couplings, and therefore they must be combined with the contributions of the same order in $V_1^{(2)}(\varphi, T)$. However, the combined result does not solve any of our previous problems related to the scalar sector, but rather introduces a new problem, the appearance of a very disturbing linear term in the effective potential. The fact that the two-loop diagrams yield terms of order g^3 and $\lambda^{3/2}$, and not only g^4 and λ^2 is another manifestation of the infrared problems in finite-temperature field theories. The two-loop contributions can be considered as one-loop graphs where the other loop plays the role of a self-energy insertion. The infrared divergencies are cut off by these dynamically generated masses (proportional to g or $\sqrt{\lambda}$), which leads to factors T/m_i and thereby reduces the order in g or λ of the corresponding diagram.

In appendix A we show that to order g^3 and $\lambda^{3/2}$ only ring diagrams contribute (cf. fig. 3). The complete summation of these terms with the proper combinatoric factors is required to obtain the correct effective potential to order g^3 and $\lambda^{3/2}$. Therefore, we need the self-energy terms at zero external momentum. The evaluation of these contributions is straightforward for scalar fields, but for vector fields the polarisation tensor needs special attention in spontaneously broken gauge theories. The next section is addressed to this question.

3 The structure of the gauge boson propagator

Most of the results of this section have already been discussed in ref. [8]. Nevertheless, they are included here to make our paper self-contained.

In order to determine the plasma masses of vector and scalar fields, we first have to discuss the structure of the vector propagator at finite temperature. The gauge boson self-energy $\Pi_{\mu\nu}(k)$ depends on the 4-momentum k^μ

and the 4-vector $u^\mu = (1, \vec{0})$ which specifies the rest frame of the system (cf. ref. [19]). Hence, in general $\Pi_{\mu\nu}$ is a linear combination of four tensors. A convenient choice is

$$P_{T\mu\nu} = g_{\mu}^i \left(\delta_{ij} - \frac{k_i k_j}{\vec{k}^2} \right) g^j{}_\nu, \quad (17)$$

$$P_{L\mu\nu} = \frac{k_\mu k_\nu}{k^2} - g_{\mu\nu} - P_{T\mu\nu} = \frac{k^2}{\vec{k}^2} u_\mu^T u_\nu^T, \quad (18)$$

$$P_{G\mu\nu} = -\frac{k_\mu k_\nu}{k^2}, \quad (19)$$

$$S_{\mu\nu} = \frac{1}{\sqrt{2\vec{k}^2}} \left(k_\mu u_\nu^T + k_\nu u_\mu^T \right), \quad (20)$$

where $u_\mu^T = u_\mu - k_\mu \frac{u \cdot k}{k^2}$ is transverse, $u_\mu^T k^\mu = 0$. These tensors satisfy the relations

$$P_T^2 = -P_T, \quad P_L^2 = -P_L, \quad P_G^2 = -P_G, \quad S^2 = \frac{1}{2}(P_L + P_G), \quad (21)$$

$$P_T P_L = P_T P_G = P_L P_G = S P_T = P_L S P_L = 0, \quad (22)$$

$$P_{T\mu}{}^\mu = 2P_{L\mu}{}^\mu = 2P_{G\mu}{}^\mu = -2, \quad S_{\mu}{}^\mu = P_{L\mu}{}^\nu S_\nu{}^\mu = 0. \quad (23)$$

In Landau gauge, where the bare propagator is transverse,

$$D(k) = \frac{-1}{k^2 - m^2} (P_L + P_T), \quad (24)$$

the gauge-boson self-energy tensor

$$\Pi(k) = \Pi_L(k) P_L + \Pi_T(k) P_T + \Pi_S(k) S + \Pi_G(k) P_G \quad (25)$$

yields the full propagator

$$\begin{aligned} \tilde{D}(k) &= \sum_{n=0}^{\infty} D(k) [\Pi(k) D(k)]^n \\ &= \frac{-1}{k^2 - m^2 - \Pi_L(k)} P_L + \frac{-1}{k^2 - m^2 - \Pi_T(k)} P_T. \end{aligned} \quad (26)$$

Due to the relations (21) and (22) the full propagator does not depend on $\Pi_S(k)$ and $\Pi_G(k)$.

However, knowledge of Π_G is important since it enters in the relations which yield the longitudinal and transverse plasma masses:

$$\delta m_L^2 = \Pi_L(0) = \text{Tr}[\Pi(0)P_L] = -\Pi_{00}(0), \quad (27)$$

$$\begin{aligned} \delta m_T^2 &= \Pi_T(0) = \frac{1}{2}\text{Tr}[\Pi(0)P_T] \\ &= -\frac{1}{2}[\Pi^\mu{}_\mu(0) + \Pi_L(0) + \Pi_G(0)] , \end{aligned} \quad (28)$$

where

$$\Pi_G(k) = \text{Tr}[\Pi(k)P_G]. \quad (29)$$

Here $\Pi_{\mu\nu}(0)$ is defined by setting first $k_0 = 0$ and then performing the limit $\vec{k}^2 \rightarrow 0$. In gauge theories with unbroken symmetry one has $\Pi_G = 0$ in Landau gauge. Note, that this is not the case if the symmetry is spontaneously broken. As eq. (28) shows this fact, which seems to have gone unnoticed in the literature, is important in order to extract the correct transverse mass from $\Pi_{\mu\nu}$. As we will see, in non-abelian gauge theories this transverse mass turns out to contain a field independent magnetic plasma mass which plays an important role in the estimation of the higher order effects. Hence, the unambiguous determination of this term is needed.

4 The effective potential in next-to-leading order

A. Ring summation

The one-loop gauge boson self-energy corrections for the $SU(2)$ gauge theory are shown in fig. (4). The self-energy contributions have very complicated dependence on the momentum $(k_0, |\vec{k}|)$. As we show in appendix A, to order g^3 and $\lambda^{3/2}$ one has to set $k_0 = 0$ for the external lines of the self-energy diagrams in the ring summation. On the other hand, by use of a Taylor expansion in $|\vec{k}|$ it is easy to show that only the $|\vec{k}| \rightarrow 0$ limit of the self-energy graphs contribute to the effective potential in this order. In this limit we find for the longitudinal and transverse plasma masses to order g^3 and $\lambda^{3/2}$:

$$\delta m_L^2 = \frac{11}{6}g^2T^2 - \frac{g^2}{16\pi} \left(\frac{4m^2}{m + \bar{m}_\varphi} + \bar{m}_\varphi + 3\bar{m}_\chi + 16m \right) T, \quad (30)$$

$$\delta m_T^2 = \frac{g^2 T}{3\pi} m - \frac{g^2}{6\pi} \left(\frac{m^2}{m + \bar{m}_\varphi} - \frac{1}{8} \frac{(\bar{m}_\varphi - \bar{m}_\chi)^2}{\bar{m}_\varphi + \bar{m}_\chi} \right) T. \quad (31)$$

Here we have neglected terms of higher order in the high-temperature expansion, since we will not need the corresponding terms in the effective potential. It is worth mentioning that no field independent transverse plasma mass appears in eq. (31), in accord with the well-known fact that in one-loop order it vanishes in all gauges. Having also determined the corresponding scalar self-energy contributions, one can perform the ring summation. The corresponding diagrams are shown in fig. 3 where the "blobs" stand for one-loop self-energy contributions (cf. fig. 4 and similar scalar terms). Special care is needed with respect to the infrared limit and the combinatoric factors, particularly in the case of one self-energy insertion, since these graphs are two-loop diagrams with different symmetries depending on the type of propagators. The ring summation yields the potential

$$V_{ring}(\varphi, T) = \frac{1}{2} \left(\frac{3g^2}{16} + \frac{\lambda}{2} + \frac{1}{4} f_t^2 \right) (T^2 - T_b^2) \varphi^2 + \frac{\lambda}{4} \varphi^4 - (3m_L^3 + 6m_T^3 + m_\varphi^3 + 3m_\chi^3) \frac{T}{12\pi} + \mathcal{O}(g^4, \lambda^2, f_t^4), \quad (32)$$

where T_b is given by eq. (14) and the masses are the sum of tree-level terms and one-loop self-energy corrections to order g^2 and λ

$$\begin{aligned} m_L^2 &= \frac{11}{6} g^2 T^2 + \frac{g^2 \varphi^2}{4}, \\ m_T^2 &= \frac{g^2 \varphi^2}{4}, \\ m_\varphi^2 &= \left(\frac{3}{16} g^2 + \frac{\lambda}{2} + \frac{1}{4} f_t^2 \right) (T^2 - T_b^2) + 3\lambda \varphi^2, \\ m_\chi^2 &= \left(\frac{3}{16} g^2 + \frac{\lambda}{2} + \frac{1}{4} f_t^2 \right) (T^2 - T_b^2) + \lambda \varphi^2. \end{aligned} \quad (33)$$

The potential (32) describes a first-order phase transition, since there exist two degenerate minima at a critical temperature T_c , similar to the case considered in sect. 2. However, due to the non-vanishing longitudinal plasma mass the strength of the transition is less than the high-temperature expansion of the one-loop result suggests. Clearly, a non-zero field independent magnetic mass m_T would further weaken the transition.

The potential (32) contains no term linear in φ . Hence, the linear terms which appear in the two-loop expression are cancelled by contributions from the ring summation. As we show in appendix A the result (32) contains all terms of order g^3 and $\lambda^{3/2}$. Therefore the appearance of linear terms of order g^3 or $\lambda^{3/2}$ can be ruled out. To higher order in g and λ the absence of a linear term has not yet been proven. Note, that for temperatures above the barrier temperature T_b all masses, and therefore also the potential, are real.

Formal arguments concerning the existence or nonexistence of linear terms in the framework of the perturbative expansion in the coupling constant are questionable, since such an expansion does not necessarily reflect the behaviour of the potential at the origin. As an illustration consider a hypothetical potential containing a term proportional to

$$\sqrt{g^{2n+2}T^2 + g^{2n}\varphi^2}. \quad (34)$$

This function is symmetric in φ and contains no linear term. Nevertheless, a formal expansion in powers of g gives rise to a linear term,

$$\sqrt{g^{2n+2}T^2 + g^{2n}\varphi^2} \approx g^n\varphi + \frac{g^{n+2}T^2}{2\varphi} + \mathcal{O}(g^{n+4}). \quad (35)$$

On the other hand, a potential with a term

$$\varphi\sqrt{g^{2n+2}T^2 + g^{2n}\varphi^2} \quad (36)$$

does contain a linear term which, however, is not visible in the expansion in powers of g :

$$\varphi\sqrt{g^{2n+2}T^2 + g^{2n}\varphi^2} \approx g^n\varphi^2 + g^{n+2}T^2/2 + \mathcal{O}(g^{n+4}). \quad (37)$$

The behaviour of the potential obtained by an expansion in the coupling constant does not coincide with that of the exact potential. Note, however, that in both cases the ratio of the next-to-leading term and the leading term becomes very large at $\varphi \approx 0$ which indicates that the perturbative expansion in g is not valid in this region. Because of this fact we will carefully study the effects of the higher order terms in the couplings at $\varphi \approx 0$ and close to the second non-trivial minimum of the effective potential (32).

The ring summation yields a sensible result to order g^3 and $\lambda^{3/2}$. This is rather surprising since individual terms in this sum are not well defined for

small values of φ due to the imaginary masses which appear in the scalar field propagators. This inconsistency would show up in the next higher order, i.e., g^4 and λ^2 , where all diagrams have to be added to the ring diagrams which contribute to this order.

B. Gap equations

In this subsection we shall evaluate the potential (32) in a more elegant way which will also enable us to estimate higher order corrections to our result. For small values of φ the temperature dependent plasma mass corrections $\delta m_{L,T}^2$ can become larger than the tree-level mass m^2 . This suggests an improved perturbation theory [2, 21], where loop diagrams are evaluated with boson propagators containing the exact masses $m_{L,T}^2 = m^2 + \delta m_{L,T}^2$, $m_{\varphi,\chi}^2 = \bar{m}_{\varphi,\chi}^2 + \delta m_{\varphi,\chi}^2$. The radiative corrections are treated as counter terms

$$\begin{aligned} \delta S_\beta = & -\frac{1}{2} \int_\beta dp \left[\tilde{A}^\mu(p) (\delta m_L^2 P_{L\mu\nu} + \delta m_T^2 P_{T\mu\nu}) \tilde{A}^\mu(p) \right. \\ & \left. - \delta m_\varphi^2 \tilde{\varphi}^2(p) - \delta m_\chi^2 \tilde{\chi}^2(p) \right], \end{aligned} \quad (38)$$

and are determined self-consistently by solving gap equations at the corresponding loop order. As it was pointed out above, there is no need to use this procedure for fermions, since fermions do not suffer from infrared problems. The ghost propagator remains massless in Landau gauge. Therefore, in our approach the bare fermion and ghost propagators play the role of full propagators. The one-loop contributions to the effective potential with these dressed propagators are shown in fig. 5. Note, that here and in the following the blobs stand for exact masses and not only for one-loop self-energy insertions. The mass counter terms for top-quark and ghost are zero.

The relevant one-loop graphs for the gap equations are shown in fig. 6. A rather lengthy, but straightforward calculation yields the following set of equations to order g^3 and $\lambda^{3/2}$:

$$m_L^2 = \frac{11}{6} g^2 T^2 + m^2 - \frac{g^2}{16\pi} \left(\frac{4m^2}{m_L + m_\varphi} + m_\varphi + 3m_\chi + 16m_T \right) T, \quad (39)$$

$$m_T^2 = \frac{g^2 T}{3\pi} m_T + m^2 - \frac{g^2}{6\pi} \left(\frac{m^2}{m_T + m_\varphi} - \frac{1}{8} \frac{(m_\varphi - m_\chi)^2}{m_\varphi + m_\chi} \right) T, \quad (40)$$

$$m_\varphi^2 = \left(\frac{3g^2}{16} + \frac{\lambda}{2} + \frac{1}{4} f_t^2 \right) (T^2 - T_b^2) + 3\bar{m}^2$$

$$\begin{aligned}
& -\frac{3g^2}{16\pi} \left[m_L + 2m_T + m^2 \left(\frac{1}{m_L} + \frac{2}{m_T} \right) \right] T \\
& -\frac{3\lambda}{4\pi} \left[m_\varphi + m_\chi + \bar{m}^2 \left(\frac{3}{m_\varphi} + \frac{1}{m_\chi} \right) \right] T,
\end{aligned} \tag{41}$$

$$\begin{aligned}
m_\chi^2 &= \left(\frac{3g^2}{16} + \frac{\lambda}{2} + \frac{1}{4}f_t^2 \right) (T^2 - T_b^2) + \bar{m}^2 \\
& -\frac{3g^2}{16\pi} (m_L + 2m_T) T \\
& -\frac{\lambda}{4\pi} \left(m_\varphi + 5m_\chi + \frac{4\bar{m}^2}{m_\varphi + m_\chi} \right) T,
\end{aligned} \tag{42}$$

where

$$m = g\varphi/2, \quad \bar{m} = \sqrt{\lambda}\varphi, \quad T_b^2 = \frac{16\lambda v^2}{3g^2 + 8\lambda + 4f_t^2}. \tag{43}$$

As already mentioned, the ghost mass remains zero, and the mass corrections for fermions are not important since their Matsubara frequencies are always at least $\mathcal{O}(1) \cdot T$. Thus, there is no need to consider gap equations for fermions and ghosts.

It is instructive, first to consider the gap equations for the pure scalar theory ($g = 0$, $f_t = 0$) at $\varphi = 0$. From eqs. (41) and (42) one obtains for temperatures close to the barrier temperature

$$m_\varphi \sim m_\chi \sim (T - T_b), \tag{44}$$

i.e., m_φ and m_χ approach zero with critical index one. This well-known result was first obtained by Dolan and Jackiw in the large- N limit [2]. We obtain the same result, because at $\varphi = 0$ only graphs e) and l) of fig. 6 contribute, which are the leading terms in the $1/N$ -expansion.

Of particular interest is eq. (40) for the magnetic mass. At $\varphi = 0$, one has $m_\varphi = m_\chi$, and therefore

$$m_T^2 = \frac{g^2 T}{3\pi} m_T. \tag{45}$$

This equation has two solutions,

$$m_T = 0, \tag{46}$$

and

$$m_T = \frac{g^2 T}{3\pi}, \quad (47)$$

thus an unwanted ambiguity seems to appear. However, only the second solution is physical, since only $m_T = g^2 T/(3\pi)$ can be continuously connected to a positive solution of eq. (40) at $\varphi > 0$. The $\varphi \rightarrow 0$ limit of the negative solution of eq. (40) is $m_T = 0$. This negative solution is unphysical, since m_T is defined as absolute value of a square root appearing in the high temperature expansion. The result (47) has been independently derived in ref. [9].

The obtained value $m_T = g^2 T/(3\pi)$ for the transverse plasma mass goes beyond the accuracy of our calculation which is only valid to order g . However, the appearance of a magnetic mass of order g^2 is expected to be a nonperturbative feature of the theory [22]. In order to study the dependence of our results on the unknown value of the magnetic mass we will take $m_T = \gamma g^2 T/(3\pi)$ as the $\varphi \rightarrow 0$ limit.

It is well known that in the abelian Higgs model the transverse plasma mass is zero at finite temperature, which is in agreement with our previous results [8]. In nonabelian gauge theories the situation is different. In this case the gauge boson self-couplings (cf. figs. 6q, 6u) yield a non-vanishing transverse plasma mass. This magnetic mass can be self-consistently determined by summing an infinite set of diagrams. The non-zero solution (47) for the transverse plasma mass can be viewed as a result of an infinite iteration process with an arbitrarily small initial value. In a diagrammatic picture the iterative solution corresponds to an infinite sum over "superdaisy"-type self-energy insertions. The appearance of a magnetic mass term has been studied by other methods in finite-temperature QCD [23]. Lattice $SU(2)$ models and infinite summations also give values for γ which are $\mathcal{O}(1)$.

Let us now solve the gap equations, which represent a set of nonlinear equations with four variables:

$$\mathcal{M}^2 = f(\mathcal{M}), \quad \mathcal{M} = (m_L, m_T, m_\chi, m_\varphi), \quad \mathcal{M}^2 = (m_L^2, m_T^2, m_\chi^2, m_\varphi^2). \quad (48)$$

Except for linear problems, finding of roots invariably proceeds by iteration. Starting from some approximate solution, a useful algorithm will improve its accuracy. We are interested in a Taylor-expansion in g and $\sqrt{\lambda}$ of the result. Setting $g = \sqrt{\lambda} = 0$ gives zero for \mathcal{M} , thus the Taylor expansion for \mathcal{M} starts with g or $\sqrt{\lambda}$, and for \mathcal{M}^2 with g^2 or λ . Suppose that we know the results for

\mathcal{M} to order n . Inserting this trial solution in the right-hand-side of the gap equations we obtain an expression to order $n+2$ for \mathcal{M}^2 , and to order $n+1$ for \mathcal{M} . The coefficients of the previous orders do not change. Consequently, the above iterative procedure reproduces the Taylor-expansion of the exact solution order by order.

This iterative solution has a diagrammatical picture. The lowest order result corresponds to the one-loop self-energy insertion at zero external momentum. A new iteration means one order higher in the coupling, e.g., the sum of the one-loop self-energy insertions of the one-loop self-energy insertion, the so-called "daisy" graphs, the next order gives a new self-energy insertion on the bare lines, and so on and so forth. After an infinite number of iterations one obtains the sum of all "superdaisy" diagrams [2]. Note, however, that this summation does not give the correct answer for the effective potential to order g^4 , λ^2 and higher. One cannot justify the zero external momentum limit of the gap equations for higher order contributions (cf. appendix A).

Our goal is to calculate the effective potential to order g^3 and $\lambda^{3/2}$. Due to the global $SU(2)$ symmetry of the theory the potential is only a function of $\sqrt{2\Phi^\dagger\Phi} = \sqrt{\varphi^2 + \chi_1^2 + \chi_2^2 + \chi_3^2}$. Hence, at $\chi = 0$, the masses $m_\varphi(\varphi, T)$ and $m_\chi(\varphi, T)$ are given by

$$m_\varphi^2(\varphi, T) = \frac{\partial^2 V(\varphi, T)}{\partial \varphi^2}, \quad (49)$$

$$m_\chi^2(\varphi, T) = \frac{1}{\varphi} \frac{\partial V(\varphi, T)}{\partial \varphi}. \quad (50)$$

Thus, in order to obtain the potential to order g^3 and $\lambda^{3/2}$ one has to evaluate m_χ or m_φ to the same order. This means two successive self-energy insertions, which is exactly the ring summation. The result reads:

$$\begin{aligned} V_{gap}(\varphi, T) &= \int_0^\varphi d\varphi' \varphi' m_\chi^2(\varphi', T) \\ &= \frac{1}{2} \left(\frac{3g^2}{16} + \frac{\lambda}{2} + \frac{1}{4} f_t^2 \right) (T^2 - T_b^2) \varphi^2 + \frac{\lambda}{4} \varphi^4 \\ &\quad - \left(3m_L^{(1)3} + 6m_T^{(1)3} + m_\varphi^{(1)3} + 3m_\chi^{(1)3} \right) \frac{T}{12\pi} \\ &\quad + \mathcal{O}(g^4, \lambda^2, f_t^4), \end{aligned} \quad (51)$$

where the lowest order masses are

$$\begin{aligned}
m_L^{(1)2} &= \frac{11}{6}g^2T^2 + m^2, \\
m_T^{(1)2} &= \gamma^2 \frac{1}{9\pi^2}g^4T^2 + m^2, \\
m_\varphi^{(1)2} &= \left(\frac{3}{16}g^2 + \frac{\lambda}{2} + \frac{1}{4}f_t^2\right)(T^2 - T_b^2) + 3\bar{m}^2, \\
m_\chi^{(1)2} &= \left(\frac{3}{16}g^2 + \frac{\lambda}{2} + \frac{1}{4}f_t^2\right)(T^2 - T_b^2) + \bar{m}^2.
\end{aligned} \tag{52}$$

As it should be, this result is identical with the ring potential (32) for $\gamma = 0$. In order to illustrate the dependence of our results on the unknown value of the magnetic mass we have modified the iterative solution of the gap equations to leading order in the couplings in such a way that $m_T^{(1)}(\varphi = 0) = \gamma g^2 T / (3\pi)$.

The evaluation of the effective potential to order g^4 , λ^2 and f_t^4 requires the incorporation of two-loop contributions in eqs. (39) - (42), and in order to obtain the exact effective potential one has to solve the full Dyson-Schwinger equations, a non-trivial task! However, the obtained gap equations already contain some part of the higher order terms, namely the "superdaisy" diagrams, and thus contain valuable information about higher order corrections. Before we investigate these questions in the next section, we study some properties of the obtained potential (51).

C. Plasma masses and the order of the phase transition

A nice feature of the one-loop effective potential considered in sect. 2, with or without cubic term, was the possibility to study the phase structure analytically. Due to the plasma masses our potential (32) or (51) now contains terms of the form $(C^2 + \varphi^2)^{3/2}$, and is therefore more complicated. Nevertheless, it is still possible to study its main properties analytically.

In order to understand the effect of plasma masses consider a hypothetical potential with one plasma mass term proportional to T ,

$$V_{hyp}(T, \varphi) = \frac{a}{2}(T^2 - T_b^2)\varphi^2 - \frac{bT}{3}(c^2T^2 + \varphi^2)^{3/2} + \frac{\lambda}{4}\varphi^4, \tag{53}$$

where a, b, c and λ are positive real numbers, independent of temperature. V_{hyp} has a local minimum at the origin as long as its second derivative there

is positive. This condition yields a corrected barrier temperature \tilde{T}_b ,

$$\tilde{T}_b^2 = \frac{T_b^2}{1 - bc/a}. \quad (54)$$

The phase transition described by this potential is first-order if at the barrier temperature \tilde{T}_b a second minimum exists at non-zero φ , otherwise it is second-order. The condition that at \tilde{T}_b the first derivative of the potential with respect to φ vanishes at some value $\varphi > 0$ implies for the couplings

$$\lambda < \frac{b}{2c}. \quad (55)$$

In the standard model only the parameter a depends on the top-quark Yukawa coupling, hence this condition does not depend on the top mass. Clearly, it implies that at a critical value of the Higgs mass the transition changes from first-order to second-order. It is easy to show that for several plasma mass terms of the form

$$\frac{b_1 T}{3}(c_1^2 T^2 + \varphi^2)^{3/2} + \frac{b_2 T}{3}(c_2^2 T^2 + \varphi^2)^{3/2} + \dots + \frac{b_n T}{3}(c_n^2 T^2 + \varphi^2)^{3/2} \quad (56)$$

the condition (55) for a first-order phase transition becomes

$$\lambda < \frac{b_1}{2c_1} + \frac{b_2}{2c_2} + \dots + \frac{b_n}{2c_n}. \quad (57)$$

If one neglects in the electroweak potential (32) terms of order $\lambda^{3/2}$, thus assuming $g^2 \gg \lambda$, the cubic term with longitudinal plasma mass is sufficient to give a first-order transition if $m_H < 13 \text{ GeV}$. However, because of the second cubic term with zero plasma mass the phase transition is first-order for all Higgs masses. This situation changes if a transverse plasma mass is included, as in eq. (51). The corresponding term in the effective potential yields a second-order transition if

$$m_H > \frac{85 \text{ GeV}}{\sqrt{\gamma}}. \quad (58)$$

Inclusion of the cubic term with longitudinal plasma mass slightly relaxes this bound according to condition (57). As already mentioned, $\gamma = O(1)$.

The scalar part of the electroweak potential needs a different treatment. Set $g = 0$. Now the potential is of the form

$$\begin{aligned} \tilde{V}_{hyp}(T, \varphi) = & \frac{a}{2}(T^2 - T_b^2)\varphi^2 + \frac{\lambda}{4}\varphi^4 - \frac{b}{9}\left(3(a(T^2 - T_b^2) + \lambda\varphi^2)^{3/2}\right. \\ & \left.+ (a(T^2 - T_b^2) + 3\lambda\varphi^2)^{3/2}\right)T, \end{aligned} \quad (59)$$

and the temperature, where the potential barrier vanishes, is

$$\tilde{T}_b^2 = \frac{T_b^2}{1 - 4b^2\lambda^2/a}. \quad (60)$$

The only solutions of the equation $\partial\tilde{V}_{hyp}(\tilde{T}_b, \varphi)/\partial\varphi = 0$ are

$$\varphi^2 = 0, \quad \varphi^2 = b\lambda\tilde{T}_b^2(-4 \pm i), \quad (61)$$

i.e., the scalar part of our potential always yields a second-order phase transition, independent of the value of λ .

In the general case of non-zero plasma masses for vector and scalar bosons (cf. eq. (51)), the order of the phase transition changes at a critical Higgs mass which can be evaluated as function of γ . The result is shown in fig. (7). Note, that for the present lower experimental bound on the Higgs mass the phase transition is always second-order for $\gamma > 2.5$.

As we shall discuss in detail in the next section, also the improved perturbative approach becomes inapplicable close to the barrier temperature. Therefore, we cannot calculate the effective potential at this temperature. Nevertheless, many features of our numerical analysis will be very similar to the result of our analytical study in this section, which one may expect based on continuity arguments.

5 Higher order effects

In this section we will estimate the size of different higher order corrections to the effective potential (51). First we will use an extended version of the method discussed in ref. [8] to check the convergence of the perturbation series. We will then study effects of a non-vanishing magnetic mass, in particular its influence on the surface tension, and finally we will perform an analysis including some higher order terms in the effective potential.

A. Convergence of the perturbation series

At the origin, $\varphi = 0$, the curvature of the potential $m_\varphi^2(0, T)$ reads (cf. eq.(41))

$$m_\varphi^2 = \left(\frac{3}{16}g^2 + \frac{\lambda}{2} + \frac{1}{4}f_t^2 \right)(T^2 - T_b^2) - \frac{3g^3}{16\pi} \sqrt{\frac{11}{6}} T^2 - \frac{3\lambda T}{2\pi} \sqrt{\left(\frac{3}{16}g^2 + \frac{\lambda}{2} + \frac{1}{4}f_t^2 \right)(T^2 - T_b^2)} \quad , \quad (62)$$

and the condition of vanishing curvature, $m_\varphi^2(0, T_b') = 0$, yields the corrected barrier temperature

$$T_b'^{-2} = \frac{1}{16\lambda v^2} \left(3g^2 + 8\lambda + 4f_t^2 - \frac{\sqrt{66}}{2\pi} g^3 + \mathcal{O}(g^4, \lambda^2, f_t^4) \right). \quad (63)$$

Note, that there is no correction of order $\lambda^{3/2}$.

At $\varphi > 0$, the gap equations (39) - (42) contain terms proportional to T/m_i which reflect the expected infrared problems of finite-temperature perturbation theory. The perturbative expansion is reliable if these terms are smaller than leading-order terms. Inspection of eqs. (39) - (42) shows that this is guaranteed if the following inequalities are satisfied:

$$\xi \frac{g^2}{6\pi} \frac{T}{m_T + m_\varphi} \leq 1 \quad , \quad (64)$$

$$\xi \frac{\lambda T}{4\pi} \left(\frac{3}{m_\varphi} + \frac{1}{m_\chi} \right) \leq 1 \quad . \quad (65)$$

The first inequality stems from the equation for m_T^2 and the second from the equation for m_φ^2 . We have included a factor ξ which ensures that leading terms of order g^2 and λ are ξ times larger than next-to-leading contributions. Clearly, for fixed values of g, λ, f_t, T and φ , the larger the value of ξ , the better the behaviour of the perturbative expansion. If the conditions (64) and (65) are satisfied one expects the uncertainty of the field dependent part of the effective potential (51) to be of order $1/\xi^2$. We will now study the implications of the above conditions in two ways. First we will use the iterative solution of the gap equations and insert the squared plasma masses

to order g^2 and λ (cf. eq. (52)) into the conditions (64) and (65). We will then repeat the analysis in a more conservative way by using the squared plasma masses in the ξ -conditions to order g^3 and $\lambda^{3/2}$, which are smaller than the ones to leading order (cf. eq. (49)).

Close to the origin, at $\varphi \approx 0$, the above conditions imply that one cannot even reach the barrier temperature T'_b . For $\gamma = 0$ eqs. (52), (64) and (65) yield the lower bounds on the temperature T ,

$$T > T_V \quad , \quad T > T_S \quad , \quad (66)$$

where

$$\frac{T_V^2 - T_b^2}{T_V^2} = \frac{\xi_V^2 g^4}{36\pi^2(\frac{3}{16}g^2 + \frac{\lambda}{2} + \frac{1}{4}f_t^2)} \quad (67)$$

and

$$\frac{T_S^2 - T_b^2}{T_S^2} = \frac{\xi_S^2 \lambda^2}{3\pi^2(\frac{3}{16}g^2 + \frac{\lambda}{2} + \frac{1}{4}f_t^2)} . \quad (68)$$

Here, the subscript “ V ” (“ S ”) indicates that the infrared divergence for the vector (scalar) field plasma mass sets the temperature. Hence, our expression for the effective potential is only reliable for temperatures above T^* , which denotes the largest temperature among T'_b, T_V and T_S . Non-zero values of γ give a non-zero magnetic mass m_T at $\varphi \approx 0$. The corresponding infrared behaviour leads to a smaller temperature T_V .

In order to establish the existence of a first-order phase transition for a given value of the scalar self-coupling λ we have to show that for some values $\varphi > 0$, where the ξ -conditions (64) and (65) are satisfied,

$$V(\varphi, T^*) \leq V(0, T^*) . \quad (69)$$

Note, that $T^* = T^*(g, \lambda)$, and thus the ξ -conditions are satisfied at $\varphi = 0$. The larger the Higgs mass, i.e., the scalar self-coupling λ , the more difficult it is to fulfill the condition for ξ_S . Let us now consider the potential in a region $\varphi > 0$, where the ξ -conditions are satisfied. At a certain maximal value of λ , and a corresponding critical temperature T_c^* , the minimum of the potential in this region, at $\varphi_* > 0$, is degenerate with the minimum at $\varphi = 0$,

$$V(\varphi_*, T_c^*) = V(0, T_c^*) . \quad (70)$$

Note, that in general $T_c^*(g, \lambda) \leq T_c(g, \lambda)$, the true critical temperature, and $\varphi_*(g, \lambda) \geq \varphi_c(g, \lambda)$, the local minimum at T_c . Hence, φ_* is not necessarily an

extremum of the potential with respect to the full range in φ . As discussed above, the condition $T^* = T_c^*$ defines a maximal value of λ for a given value of ξ . We have plotted the corresponding functions $m_H(\xi_S)$ and $m_H(\xi_V)$ in fig. 8. The condition obtained from the gauge boson gap equation is always satisfied with $\xi_V \geq 7.6$, even for $\gamma = 0$. The result is essentially independent of the top mass in the range $m_t = 110 - 180 \text{ GeV}$. Both, ξ_V and ξ_S are larger than 2 up to Higgs masses of approximately 200 GeV .

Let us now repeat this analysis using the higher order plasma masses (49) in the ξ -conditions. The allowed minimal temperature T^* is higher than in the previous case. Since the Goldstone mass $m_\chi^2 = 2\partial V/\partial\varphi^2$ vanishes at the second minimum $\varphi(T^*)$, the condition (65) cannot be satisfied here and the perturbative approach breaks down. Hence, one always has $\varphi_* > \varphi(T^*)$. We can now determine the temperatures $T^*(g, \lambda)$. In order to illustrate how far T_c^* lies below the true critical temperature T_c , we have plotted an effective potential at T_c^* in fig. 9. The condition $T^*(g, \lambda) = T_c^*(g, \lambda)$ again defines a line in the ξ - λ -plane, denoted by ξ'_S in fig. 8. The difference between the two boundaries ξ_S and ξ'_S in fig. 8 is considerable. For Higgs masses above 80 GeV the value of ξ'_S is smaller than 2.

B. The effect of a magnetic mass

Our estimate of the largest Higgs mass up to which perturbation theory is reliable, which we have carried out in the previous subchapter, depends on the parameter ξ . The appropriate value of ξ can only be determined by calculating higher order corrections. In sect. 4C we saw that the magnetic mass has an important effect on the phase transition. Hence, the effective potential has to be calculated at least up to terms proportional to g^6 , the order at which the magnetic mass contributes. Since we have not calculated all graphs contributing to this order, we have introduced a constant γ in eqs. (52) which parameterizes the uncertainty in the size of the magnetic mass. The solution of our gap equations gives $\gamma = 1$, other approaches (cf. ref. [23]) yield values of the same order of magnitude.

In order to estimate the effect of the magnetic mass on the phase transition we calculate the surface tension, a physical quantity, from the potential (51) as function of λ and γ :

$$\sigma(\lambda, \gamma) = \int_0^{\varphi_c} d\varphi \sqrt{2V(\varphi, T_c)}, \quad \varphi_c = \varphi(T_c). \quad (71)$$

As discussed in the previous section, the temperature T_c is always larger than the temperature T_c^* , if the chosen value of λ is allowed by the value chosen for ξ . Therefore one can reliably calculate the potential close to the origin, $\varphi \approx 0$, and for large values of φ . Of course, in the intermediate regime, which is needed in order to get the surface tension from eq. (71), the potential has large uncertainties. Nevertheless, as the dominant contribution comes from the vector loops which have no infrared problems in the intermediate range of φ , it is conceivable that the surface tension, which is an integrated quantity, can be obtained from eqs. (51) and (71) to good approximation.

We have plotted σ as function of the Higgs mass for different values of γ in fig. 10. Note, that the disappearance of the surface tension means transition to a second-order phase transition. The Higgs masses for which σ vanishes for different values of γ are in agreement with fig. 7. For a given value of m_H the effect of the magnetic mass on the phase transition can be characterised by the ratio

$$\zeta(\gamma) = 1 - \frac{|\sigma(m_H, \gamma) - \sigma(m_H, 0)|}{\sigma(m_H, \gamma) + \sigma(m_H, 0)}. \quad (72)$$

Clearly, if $\zeta(\gamma) \ll 1$ unknown higher order corrections are so large that a first-order phase transition cannot be established unequivocally. According to fig. 10 the quantity ζ is of $\mathcal{O}(1)$ for Higgs masses up to about 70 GeV . This value of m_H is rather close to the present lower experimental bound.

C. Scalar loop and superdaisy contributions

In this subchapter we analyse the role of some higher order terms in the perturbative expansion. As in the previous subchapter we again study the surface tension (71).

It is instructive to first set $g = 0$ and to look at the perturbative expansion in λ . The phase transition of the pure scalar theory is well known to be second-order. Our results agree with this fact, since the effective potentials in the leading order, $\mathcal{O}(\lambda)$, and the next-to-leading order, $\mathcal{O}(\lambda^{3/2})$, give second-order phase transitions. The appearance of a first-order phase transition would only be a sign that our perturbation expansion is not reliable, since it would result from a cancellation between terms of different orders. In other words, contributions from different orders would be of the same order of magnitude.

Let us now study the case $g \neq 0$. The scalar contributions together with the term $\mathcal{O}(g^2)$ give a second-order phase transition, while inclusion of terms of order g^3 yields a first-order transition. The above mentioned problem is not relevant here, since the cancellation takes place between terms proportional to different expansion parameters, namely g^3 and λ . In this perturbative approach, where $g^3 \approx \lambda$, the size of the next-order terms (in our case $\lambda^{3/2}$ and g^4) must be small, and in particular their effect on the surface tension has to be a reasonable correction.

We have determined the contribution $\mathcal{O}(\lambda^{3/2})$ to the effective potential. In fig. 11 we have plotted the surface tension at the critical temperature as function of the Higgs mass for the potential containing terms $\mathcal{O}(\lambda^{3/2}, g^3)$ (solid line) and for the potential with terms $\mathcal{O}(\lambda, g^3)$ (long dashed line). For small Higgs masses the difference is small, but at approximately 100 GeV the difference becomes $\mathcal{O}(50\%)$ indicating a breakdown of the perturbative approach.

Superdaisy diagrams can be summed by finding exact solutions to the gap equations. Iterating the gap equations we have determined the contribution of the superdaisy diagrams to order g^4 and λ^2 . The rather lengthy expressions for the potential are given in appendix B. In fig. 11 we have plotted the surface tension at the obtained critical temperature for this effective potential (short dashed line). The superdaisy terms give a correction $\mathcal{O}(20\%)$ correction, and thus do not change the qualitative picture of a first-order phase transition.

6 Decay of metastable states

In condensed matter physics the decay of metastable states is described by Langer's theory [18]. The starting point is a coarse-grained free energy which depends on the order parameter, temperature and the coarse graining scale. As function of the order parameter the free energy has a local metastable minimum which is separated from the global minimum by a barrier whose height determines the lifetime of the metastable state. From a stationary solution of the Fokker-Planck equation for the probability distribution of large fluctuations of the order parameter ("subcritical droplets") one then obtains a formula for the decay rate [18] which depends on the free energy of the metastable state, the free energy of a saddle point field configuration which

interpolates between local and global minimum and a "dynamical factor" which cannot be obtained from equilibrium thermodynamics.

Langer's formalism can be directly applied to the decay of metastable states in quantum field theories. The case of scalar electrodynamics has been studied in a recent paper [8]. The decay rate is given by

$$\Gamma = \frac{\kappa}{2\pi} \frac{\text{Im} Z_\beta[\bar{\Phi}]}{Z_\beta[\Phi = 0]} \quad , \quad (73)$$

where

$$\begin{aligned} Z_\beta[\Phi] &= e^{-\beta F[\Phi, T]} \\ &= \int_\beta [D\hat{\Phi}][DA_\mu][D\psi] e^{-\left(S_\beta[\Phi + \hat{\Phi}, A_\mu, \psi] - \int_\beta dx \frac{\delta F[\Phi, T]}{\delta \Phi(x)} \hat{\Phi}(x)\right)}. \end{aligned} \quad (74)$$

The integration measure for the vector field includes the gauge fixing and ghost terms, and ψ stands for all fermion fields. In general, the free energy also depends on A_μ and ψ . However, we will only consider stationary points with $A_\mu = \psi = 0$. For simplicity we have therefore omitted the dependence of $F[\Phi, T]$ on A_μ and ψ as well as the corresponding functional derivative terms in the exponent of eq. (74). $\bar{\Phi}$ is a field configuration which interpolates between the symmetric and the broken phase. Since $\Phi = 0$ and $\bar{\Phi}$ are approximate stationary points of the free energy $F[\Phi, T]$, we neglect the second term of the integrand in eq. (74).

The functional integral over vector and fermion fields yields an effective action which depends on the scalar field $\Phi + \hat{\Phi}$,

$$\begin{aligned} &\int_\beta [DA_\mu][D\psi] e^{-S_\beta[\Phi + \hat{\Phi}, A_\mu, \psi]} \\ &= \exp\left(-\int_\beta dx (\partial_\mu(\Phi + \hat{\Phi})^\dagger \partial^\mu(\Phi + \hat{\Phi}) - V_0(z) \right. \\ &\quad \left. - \tilde{V}(z, T) + \tilde{Z}(z, T) \partial_\mu(\Phi + \hat{\Phi})^\dagger \partial^\mu(\Phi + \hat{\Phi}) + \dots\right), \end{aligned} \quad (75)$$

where $z = \sqrt{2(\Phi + \hat{\Phi})^\dagger(\Phi + \hat{\Phi})}$. Note, that this expression is invariant under the global symmetry $O(4)$ rather than $SU(2) \times U(1)$ which is the symmetry of the Lagrangian given in eq. (1). Indeed, integrating out the top-quark yields additional wave function correction terms $\tilde{Z}_i(\Phi + \hat{\Phi})$ which are invariant only under the smaller symmetry group. For simplicity we will neglect all wave

function correction terms in the following. A more detailed discussion will be given elsewhere [29].

At one-loop order the potential $\tilde{V}(z, T)$ is well known. Including vector boson and top quark loops one obtains for the full potential in the high temperature expansion (cf. eq.(32)):

$$\begin{aligned}\bar{V}(\varphi, T) &= V_0(\varphi) + \tilde{V}(\varphi, T) \\ &= \frac{1}{2}\left(\frac{3g^2}{16} + \frac{1}{4}f_t^2\right)(T^2 - T_b^2)\varphi^2 + \frac{\lambda}{4}\varphi^4 \\ &\quad - \frac{3g^3}{32\pi}\varphi^3 T + \mathcal{O}(g^4, f_t^4).\end{aligned}\tag{76}$$

The potential has two local minima, at $\varphi = 0$ and at $\varphi(T) > 0$. At the critical temperature T_c both minima are degenerate and one has

$$\varphi_c \equiv \varphi(T_c) = \frac{g^3}{8\pi\lambda}T_c.\tag{77}$$

The integral over the scalar field fluctuations $\hat{\Phi}$ can now be carried out in the saddle point approximation. In the thin wall approximation [24] the stationary point of the approximate free energy

$$\bar{F}[\Phi, T] = \int d^3x (|\vec{\nabla}\Phi|^2 + \bar{V}(z, T)) \quad ,\tag{78}$$

which appears in the integrand of eq. (74), has a saddle point $\bar{\Phi}$ which interpolates between $\Phi = 0$ and $\Phi(T) > 0$. For temperatures just below the critical temperature T_c the height of the barrier between the two minima is large compared to the potential difference between the minima. In this case the saddle point can be computed in the thin wall approximation and one obtains

$$\bar{\Phi}(r) = \frac{1}{\sqrt{2}}\bar{\varphi}(r) = \frac{1}{2\sqrt{2}}\varphi_c \left[1 - \tanh\left(\frac{r - R(T)}{d}\right)\right],\tag{79}$$

with

$$\begin{aligned}d &= \frac{2\sqrt{2}}{\sqrt{\lambda}\varphi_c}, \\ \sigma &= \int_0^{\varphi_c} d\varphi \sqrt{2\bar{V}(\varphi, T_c)}, \\ R(T) &= \frac{2\sigma}{\varepsilon(T)}, \quad \varepsilon(T) = \bar{V}(0, T) - \bar{V}(\varphi(T), T).\end{aligned}\tag{80}$$

The free energy $\bar{F}_{TW}[\bar{\Phi}, T]$ in this approximation is then the sum of a volume term and a surface term:

$$\bar{F}_{TW}[\bar{\Phi}, T] = 4\pi R^2(T)\sigma - \frac{4\pi}{3}R^3(T)\varepsilon(T). \quad (81)$$

It is sufficient to evaluate the surface tension σ at the critical temperature T_c .

For the partition function of the saddle point one now obtains

$$\text{Im } Z_\beta[\bar{\Phi}] = \frac{1}{\sqrt{|\bar{\lambda}_-|}} \mathcal{V} \prod_i^> (\bar{\lambda}_i)^{-1/2} e^{-\beta \bar{F}[\bar{\Phi}, T]}, \quad (82)$$

where $\prod_i^>$ denotes the product of all positive eigenvalues $\bar{\lambda}_i$ of fluctuations around $\bar{\Phi}$, $\bar{\lambda}_-$ is the single negative eigenvalue, and \mathcal{V} is the volume of zero modes associated with the symmetries of the system under consideration.

The scalar fluctuations $\hat{\Phi}$ consist of the radial modes $\hat{\varphi}$ and the Goldstone modes $\hat{\chi}_i$:

$$\begin{aligned} \bar{F}[\bar{\Phi} + \hat{\Phi}, T] &= \bar{F}[\bar{\Phi}, T] \\ &+ \frac{1}{2} \int_\beta dx \, \hat{\varphi}(x) (-\Delta + U_\varphi(r)) \hat{\varphi}(x) \\ &+ \frac{1}{2} \int_\beta dx \, \hat{\chi}_i(x) (-\Delta + U_\chi(r)) \hat{\chi}_i(y). \end{aligned} \quad (83)$$

The corresponding potentials for the scalar fields $\hat{\varphi}$ and $\hat{\chi}$ are

$$U_\varphi(r) = \frac{\partial^2}{\partial \varphi^2} \bar{V}(\varphi, T) \Big|_{\varphi=\bar{\varphi}(r)}, \quad (84)$$

$$U_\chi(r) = \frac{1}{\varphi} \frac{\partial}{\partial \varphi} \bar{V}(\varphi, T) \Big|_{\varphi=\bar{\varphi}(r)}. \quad (85)$$

The spectrum of eigenvalues contains six zero modes, three for translational invariance and three for the global $SU(2) \times U(1)$ symmetry of $\bar{F}[\Phi, T]$ which is spontaneously broken to the electromagnetic $U(1)$ subgroup. The corresponding volume factor for the translational modes is well known. The volume factor for the global symmetry can be calculated in the same way as for sphaleron tunneling processes, the details are given in appendix C. One

obtains:

$$\begin{aligned}\mathcal{V}_\varphi &= \left(\frac{\beta}{2\pi} \bar{F}_A[\bar{\Phi}, T] \right)^{3/2} V, \\ \mathcal{V}_\chi &= \frac{\pi^2}{2} \left(\frac{\beta}{2\pi} \int d^3x \bar{\varphi}^2 \right)^{3/2},\end{aligned}\tag{86}$$

where V is the total volume of the physical three dimensional space.

The discrete $\hat{\varphi}$ spectrum is well known [18, 25], since the bound states are localized at $r \approx R$. There is one negative eigenvalue,

$$\lambda_- \approx -\frac{2}{R^2},\tag{87}$$

which guarantees that $Z_\beta[\bar{\Phi}]$ is purely imaginary. Furthermore, there are “Goldstone modes” which correspond to deformations of the droplet surface [18, 25, 26]. The corresponding contribution to the determinant of eigenvalues is $(\mu R)^{-5/3}$, where $\mu = m_\varphi(0, T)$ [27]. Combining eqs. (73), (81), (86) and (87) we finally arrive at the transition rate

$$\frac{\Gamma}{V} = \frac{\sqrt{2}}{2^9 \cdot 3^3 \cdot \pi^2} \frac{g^9}{\lambda^3} \kappa (\beta\sigma)^{3/2} (\beta\mu)^{-3/2} (R\mu)^{41/6} e^{-\frac{4\pi}{3}\beta\sigma R^2}.\tag{88}$$

Here the contributions of zero modes and Goldstone modes to the determinant of scalar fluctuations around the saddle point have been taken into account. The “dynamical factor” κ has recently been evaluated [28],

$$\kappa = \frac{16\eta\sigma}{3(\Delta\omega)^2 R^3},\tag{89}$$

where $\Delta\omega$ is the difference of the enthalpy $\omega = -T\partial V/\partial T$ between symmetric and broken phase, and the viscosity $\eta = 65.4 T^3$ in the standard model [28]. The pre-factor of the exponential in eq. (88) and the naive estimate T^4 turn out to give in our numerical calculations essentially the same results. However, a priori this is not clear, and the evaluation of the pre-factor is needed to verify the validity of the semiclassical approximation.

Eq. (88) gives the decay rate of the metastable symmetric phase in the framework of Langer’s theory of metastability. The free energy $\bar{F}[\Phi, T]$, obtained by integrating out vector boson and fermion fields, plays the role of

	\bar{V}	$V_{2/3}$	V_λ	V_γ
T_c [GeV]	102	102	103	103
$T_c - T_e$ [GeV]	0.05	0.02	0.02	0.01
$T_c - T_b$ [GeV]	0.63	0.28	0.36	0.05
φ_c/T_c	0.38	0.25	0.25	0.23
σ [GeV ³]	1396	409	624	187
F/T	240	223	232	221
F_{TW}/T	143	143	143	143
R [GeV ⁻¹]	1.6	2.9	2.4	4.3
R/ξ	8	10	9	6
d/R	0.30	0.25	0.28	0.29

Table 1: Observables of the first-order phase transition for four different effective potentials, a Higgs mass of 70 GeV and a top-quark mass of 140 GeV.

the coarse-grained free energy in condensed matter physics. An important aspect of this approach is that scalar fluctuations are only computed around the stationary points $\Phi = 0$ and $\Phi = \bar{\Phi}$ of $\bar{F}_A[\Phi, T]$ and not, as usually done, around unstable homogeneous scalar background fields. Hence, the perturbative approach is consistent and does not break down due to infrared divergencies or negative scalar mass terms. The decay rate (88) is similar to the result obtained for scalar electrodynamics [8]. The difference in the pre-factor is due to the different global symmetries which are spontaneously broken.

Let us finally consider the cosmological phase transition. A rough estimate of the temperature T_e at which the phase transition ends, is obtained by requiring

$$\Gamma(t_e)t_e^4 \sim 1, \quad (90)$$

where $t \approx 0.03 \cdot m_{pl}/T^2$. As an example we choose for Higgs boson and top quark masses the values $m_H = 70 \text{ GeV}$ and $m_t = 140 \text{ GeV}$. The W-boson mass is $m_W = 80.6 \text{ GeV}$. These masses correspond to the coupling constants $\lambda = 0.04$, $f_t = 0.80$ and $g = 0.66$. From our discussion in sect. 5 we know that for these parameters higher order corrections are under control so that we can still say that the phase transition is first-order. From the free energy \bar{F} (cf. eq.(78)) we can compute the critical temperature T_c , the barrier temperature T_b , the surface tension σ , the correlation length of the symmetric phase $\xi = 1/\mu$, and the value of the Higgs field inside the droplet, i.e. φ_c/T_c . From eqs. (88) and (90) we then obtain the temperature T_e and the size of R of the critical droplet. All these quantities are listed in table 1. Note, that the size of the pre-factor in the total rate relative to the exponential is of order 1%. The thin wall approximation for the Higgs mass used in the table is marginally applicable. We have plotted \bar{V} on fig. 13 for three different Higgs masses at the corresponding temperature T_e . As it can be seen, the larger the Higgs mass the better the thin wall approximation.

How reliable are these results? Since the ratio φ_c/T_c is rather small, the longitudinal plasma mass m_L (cf. eq. (39)) is essentially independent of φ . Hence, the longitudinal degree of freedom of the vector field decouples and does not contribute to the tunneling process. This leads to a reduction of the cubic term in the effective potential by $\frac{1}{3}$ [5]. This effect is not included in the potential \bar{V} . Let us denote the potential with the reduced cubic term by $V_{\frac{2}{3}}$. As shown in table 1, the effect on the surface tension is considerable. However, the phase transition clearly remains first-order with some change in the relevant temperatures and droplet properties. In order to illustrate the possible effect of higher order corrections we have also computed the observables for the potential including the scalar loops (V_λ) and for the potential with scalar loops and a non-vanishing magnetic mass ($\gamma = 1$) (cf. eq. (51)). Note in particular the effect of the magnetic mass on the surface tension. A more detailed quantitative discussion will be presented in a separate paper [29].

To conclude, we have obtained a consistent description of a cosmological first-order electroweak phase transition for values of the Higgs boson and top-quark masses which are compatible with present experimental limits. The phase transition is only weakly first order. The quantitative description of the transition can be used as input for models of baryogenesis.

7 Summary

In the previous sections we have studied the transition from the symmetric to the broken phase in the $SU(2)$ gauge theory at finite temperature. We have seen that, due to infrared divergencies, ordinary perturbation theory to any finite number of loops does not yield a useful approximation to the effective potential. However, an improved perturbation theory, which takes plasma masses into account, describes consistently the symmetric phase ($\varphi = 0$) and also the broken phase ($\varphi > 0$) in the neighbourhood of the second non-trivial, local minimum of the effective potential. Using this improved perturbation theory we have evaluated the effective potential including all terms cubic in the couplings and shown that all contributions linear in φ cancel. To this order in the couplings the ring summation and the improved perturbative approach are equivalent.

The plasma masses have been determined from a set of one-loop gap equations. A non-vanishing transverse gauge boson plasma mass was obtained, originating from the non-abelian gauge interactions. Based on the gap equations we also found a range in the couplings g , λ and f_t , the temperature T and the scalar field φ , where the perturbative approach is reliable. The dependence on the top-quark Yukawa coupling f_t turns out to be irrelevant. Knowing this range in T and φ as function of g and λ where the effective potential is reliable has allowed us to determine the range in λ where the symmetric phase is metastable. As a criterion we required that at the origin, $\varphi = 0$, the effective potential has only a local and not a global minimum for the allowed values of T .

We find that the electroweak phase transition is weakly first-order and that our perturbative approach in fact breaks down for Higgs masses close to the present experimental lower bound. Higher order corrections from scalar loops become important for Higgs masses around 80 GeV , for vanishing magnetic mass of the W -boson (cf. sects. 4A and 4C). For non-vanishing magnetic mass ($\gamma = 1$) the perturbative approach breaks down around $m_H = 70 \text{ GeV}$.

Following the theory of Langer we have finally computed the nucleation rate for critical droplets, and we have discussed some aspects of the cosmological phase transition. Up to Higgs masses of order 80 GeV the picture of a first-order transition, which proceeds via nucleation and growth of critical droplets, appears self-consistent, if the magnetic plasma mass vanishes.

However, the thin wall approximation is only marginally applicable. Furthermore, the Higgs vacuum expectation value inside the critical droplet is much smaller than the value required by models of electroweak baryogenesis.

Our results could be improved in several respects. Clearly, a complete computation of the effective potential to order g^4 , λ^2 and f_t^4 would be very valuable in order to further test the convergence of the perturbation theory. A method to identify the relevant contributions is given in appendix A. Furthermore, the validity of the expansion in powers of derivatives used in sect. 6 has to be examined in greater detail. However, the most crucial ingredient concerning the order of the transition and the difference between abelian and non-abelian gauge theories appears to be the magnetic gauge boson mass, whose origin and size require further investigations.

We would like to thank M. Lüscher, I. Montvay, M. Reuter, N. Tetradis and C. Wetterich for helpful discussions and comments.

Appendix A Ring diagram summation

As it was promised we will now prove that only ring diagrams give non-zero contributions cubic in the couplings ($g, \sqrt{\lambda}$ and f_t).

Instead of $g, \sqrt{\lambda}$ and f_t we will use in the following a generic coupling h . The naive order of a Feynman diagram is given by

$$\mathcal{O}_{naive} = V_{naive}^{(1)} + 2V_{naive}^{(2)}, \quad (\text{A.1})$$

where $V_{naive}^{(1)}$ is the number of the vertices of order h (the triple vector vertex, the ghost-ghost-vector vertex, the scalar-scalar-vector vertex and the fermion-fermion-boson vertices) and $V_{naive}^{(2)}$ is the number of the vertices of order h^2 (the scalar triple self-coupling, the vector-vector-scalar vertex and the quartic boson vertices). We study a graph with non-zero number of vertices contributing to the effective potential. It is one-particle irreducible with no external lines. Momentum conservation gives a relationship between the total number of vertices ($V = V_{naive}^{(1)} + V_{naive}^{(2)}$), the number of independent loops (L) and internal lines (I),

$$V + L - I = 1. \quad (\text{A.2})$$

The momenta of the internal lines q_1, q_2, \dots, q_I are linear combinations of the loop variables p_1, p_2, \dots, p_L . A lower order contribution in h ($\mathcal{O} < \mathcal{O}_{naive}$) could arise if some of the Matsubara frequencies, e.g. $q_{10}, q_{20}, \dots, q_{s0}$, vanish. Denote the loop momenta with vanishing Matsubara frequencies as p_1, p_2, \dots, p_r . We call lines or loops with vanishing Matsubara frequencies soft, those with non-vanishing Matsubara frequencies hard (cf. ref. [30]). Fermions have always non-zero Matsubara frequencies, thus fermion lines and loops are always hard.

The substitution in the soft loop variables

$$\vec{p}_1 = m_1^{(L)} \vec{y}_1, \quad \vec{p}_2 = m_2^{(L)} \vec{y}_2, \quad \dots, \quad \vec{p}_r = m_r^{(L)} \vec{y}_r \quad (\text{A.3})$$

results in a similar substitution for the propagators

$$\vec{q}_1 = m_1^{(I)} \vec{x}_1, \quad \vec{q}_2 = m_2^{(I)} \vec{x}_2, \quad \dots, \quad \vec{q}_s = m_s^{(I)} \vec{x}_s. \quad (\text{A.4})$$

Here the masses are proportional to the coupling h

$$m_i^{(L \text{ or } I)} = h a_i^{(L \text{ or } I)}, \quad a_i = \begin{cases} \varphi/2 & \text{for vector boson;} \\ \sqrt{\varphi^2 - v^2} & \text{for Goldstone bosons;} \\ \sqrt{3\varphi^2 - v^2} & \text{for the Higgs boson.} \end{cases} \quad (\text{A.5})$$

The above transformation gives for each soft loop integration,

$$\int d^3 p_i = m_i^3 \int d^3 y_i \propto h^3 \int d^3 y_i, \quad (\text{A.6})$$

an additional factor of h^3 , and for each soft boson propagator,

$$D(\vec{q}_i) = \frac{1}{m_i^2} D(\vec{x}_i) \propto h^{-2} D(\vec{x}_i), \quad (\text{A.7})$$

an additional factor of h^{-2} . The same factorization can be done for vertices with momentum dependence if all of the incoming lines are soft,

$$\mathcal{W}(\vec{p}_i, \vec{p}_j, \vec{p}_k) \propto h \mathcal{W}(\vec{x}_i, \vec{x}_j, \vec{x}_k), \quad (\text{A.8})$$

where \mathcal{W} is a linear combination of the soft momenta. Note, that for the ghost-ghost-vector vertex this additional factor h appears not only in the case where all of the lines are soft, but also if one of the incoming ghost lines are soft.

Hence, inspection of the Feynman rules suggest that the diagram is at least of the order

$$\mathcal{O} = 2V^{(2)} + V^{(1)} + 3r - 2s, \quad (\text{A.9})$$

where $V^{(1)}$ is the number of the vertices with naive order h and at least two incoming hard lines.

Remove now the r soft lines from the graph and consider the remaining subdiagram containing only hard lines. This subdiagram is not necessarily connected but all of the $j = 1, \dots, n$ connected parts are closed graphs with no external lines. (The original graph has no external lines and due to the momentum conservation at the vertices there is no way to connect a hard line only to soft lines.) The relationship (A.2) is valid for each of these connected graphs with V_j vertices, L_j loops and I_j lines, thus

$$V_j + L_j - I_j = 1, \quad j = 1, \dots, n. \quad (\text{A.10})$$

Note, that in this case some of the vertices are connected only to two lines but this fact has no influence on our consideration. Clearly, the number of the vertices in the j -th connected graph V_j is the sum of the number of the vertices of order h and the number of the vertices of h^2 , thus

$$V_j = V_j^{(1)} + V_j^{(2)}. \quad (\text{A.11})$$

The sum of the hard lines in the individual connected hard subdiagrams is the total number of the hard lines $(I - s)$, and the sum of the individual hard loops is the total number of the hard loops $(L - r)$,

$$\sum_j L_j = L - r, \quad \sum_j I_j = I - s. \quad (\text{A.12})$$

Since the vertices of order h have at least two hard lines the connected hard subdiagrams contain all of them

$$\sum_j V_j^{(1)} = V^{(1)}. \quad (\text{A.13})$$

Summing (A.10) over j one obtains

$$\sum_j (V_j - 1) + (L - r) - (I - s) = 0. \quad (\text{A.14})$$

Solving for s and inserting it into (A.9) yields

$$\begin{aligned} \mathcal{O} &= 2V^{(2)} + 2V^{(1)} - V^{(1)} + r + 2r - 2s \\ &= 2V - V^{(1)} + r + 2r + 2 \left(L - r - I - \sum_j (V_j - 1) \right). \end{aligned} \quad (\text{A.15})$$

From this equation, the relation $V + L - I = 1$, (A.11) and (A.13) one obtains the final answer

$$\mathcal{O} = (2 + r) + \sum_j (V_j^{(1)} + 2V_j^{(2)} - 2). \quad (\text{A.16})$$

The case $r = 0$ corresponds to no soft lines, thus the order of the diagram is just the naive order. For $r = 1$ the order of the diagram is at least 3, where we have one soft loop. If $V_j^{(1)} + 2V_j^{(2)} - 2 = 0$ for $j = 1, \dots, n$, then the order of the graph is still 3. To ensure this for a given j there are two possibilities. Either there is only one quartic coupling of order h^2 in this hard subgraph or there are two triple vertices of order h (since we only study one-particle irreducible contributions to the effective potential it is not possible to have only one triple vertex in a hard subgraph.) These are just the ring diagrams. Note, that the self-energy insertion with two scalar triple vertices or vector-vector-scalar vertices do not belong to this class.

If one wants to collect the graphs of order h^4 one has to take into account the previous ($r = 1$) graphs one order further in the high temperature expansion, a finite number of graphs with no soft loops ($r = 0$), no new terms with one soft loop ($r = 1$) and the above mentioned hard graphs ($V_j^{(1)} + 2V_j^{(2)} - 2 = 0$) for the case with two soft loops ($r = 2$). As before, self-energy insertions to order h^2 are satisfactory.

Appendix B Partial summation of superdaisy graphs

As we have shown performing an iterative solution of the gap equations one can obtain higher order contributions to the effective potential. In this appendix we calculate the g^4 , λ^2 and f_t^4 contributions. Clearly, not all of this corrections are involved in the solution of the gap equations, because a summation where all the self-energy insertions are calculated at zero external momenta cannot be justified.

The leading order masses (52) were obtained by one iteration of the gap equations, keeping the terms of order g , $\sqrt{\lambda}$ or f_t . Inserting these masses in the gap equations and performing a Taylor expansion up to order g^2 , λ and f_t^2 in the square-roots of the obtained quantities, one gets the next order masses.

$$\begin{aligned}
m_L^{(2)} &= ga + \left(-\frac{3d}{32a} - \frac{c}{32a} - \frac{b}{2a} - \frac{\varphi^2}{32a(c+a)} \right) g^2 T \pi^{-1}, \\
m_T^{(2)} &= gb + \left(\frac{d^2}{96b(d+c)} - \frac{dc}{48b(d+c)} \right. \\
&\quad \left. + \frac{c^2}{96b(d+c)} - \frac{\varphi^2}{48b(c+b)} \right) g^2 T \pi^{-1}, \\
m_\varphi^{(2)} &= gc + \left(-\frac{3\varphi^2}{64cb} - \frac{3b}{16c} - \frac{3a}{32c} - \frac{3\varphi^2}{128ca} \right) g^2 T \pi^{-1} \\
&\quad + \left(-\frac{3d}{8c} - 3/8 \right) T \lambda \pi^{-1} \\
&\quad + \left(-\frac{3\varphi^2}{8dc} - \frac{9\varphi^2}{8c^2} \right) \lambda^2 T \pi^{-1} g^{-2}, \\
m_\chi^{(2)} &= gd + \left(-\frac{3b}{16d} - \frac{3a}{32d} \right) g^2 T \pi^{-1} + \left(-\frac{c}{8d} - 5/8 \right) T \lambda \pi^{-1} \\
&\quad - \frac{T \lambda^2 \varphi^2}{2dg^2\pi(d+c)}. \tag{B.1}
\end{aligned}$$

In order to reduce the size of our formulas a, b, c and d were introduced. They are proportional to the leading order masses. Thus,

$$a = \frac{m_L^{(1)}}{g} = \sqrt{\frac{11}{6}T^2 + \frac{\varphi^2}{4}}$$

$$\begin{aligned}
b &= \frac{m_T^{(1)}}{g} = \frac{\varphi}{2} \\
c &= \frac{m_\varphi^{(1)}}{g} = \sqrt{\left(\frac{3}{16} + \frac{\lambda}{2g^2} + \frac{f_t^2}{4g^2}\right)(T^2 - T_b^2) + 3\frac{\lambda\varphi^2}{g^2}} \\
d &= \frac{m_\chi^{(1)}}{g} = \sqrt{\left(\frac{3}{16} + \frac{\lambda}{2g^2} + \frac{f_t^2}{4g^2}\right)(T^2 - T_b^2) + \frac{\lambda\varphi^2}{g^2}}. \tag{B.2}
\end{aligned}$$

By use of this masses the next iteration with a Taylor expansion of order g^4 , λ^2 and f_t^4 can be carried out. After this straightforward but fairly tedious calculation the next order Goldstone mass term is of the form:

$$\begin{aligned}
m_\chi^{(3)^2} &= \left(-\frac{\varphi^4}{2(d+c)^3 d} - \frac{9\varphi^4}{8(d+c)^2 c^2} - \frac{3\varphi^4}{8(d+c)^2 cd} \right) \lambda^4 T^2 \pi^{-2} g^{-4} \\
&+ d^2 g^2 + \left(-\frac{\varphi^2 c}{8(d+c)^2 d} - \frac{\varphi^2}{(d+c)^2} + \frac{5\varphi^2}{8d(d+c)} \right. \\
&+ \left. \frac{9\varphi^2}{32c^2} - \frac{3\varphi^2 d}{8(d+c)^2 c} + \frac{3\varphi^2}{32cd} \right) \lambda^3 T^2 \pi^{-2} g^{-2} \\
&+ \left(\frac{15b}{64d} + \frac{3a}{128c} + \frac{3b}{64c} + \frac{3\varphi^2}{256cb} + \frac{3\varphi^2}{512ca} + \frac{15a}{128d} \right) \lambda T^2 g^2 \pi^{-2} \\
&- \frac{T\lambda^2 \varphi^2}{g\pi(d+c)} + \frac{\left(-\frac{c}{4} - \frac{5d}{4}\right) \lambda T g}{\pi} + \frac{\left(-\frac{3a}{16} - \frac{3b}{8}\right) T g^3}{\pi} \\
&+ \left(-\frac{d^2}{256b(d+c)} + \frac{3b}{32a} + \frac{9d}{512a} + \frac{cd}{128b(d+c)} - \frac{c^2}{256b(d+c)} \right. \\
&+ \left. \frac{3c}{512a} + \frac{3\varphi^2}{512a(c+a)} + \frac{\varphi^2}{128b(c+b)} \right) T^2 g^4 \pi^{-2} \\
&+ \left(-\frac{3\varphi^2 a}{32(d+c)^2 c} - \frac{3\varphi^2 b}{16(d+c)^2 d} - \frac{3\varphi^4}{128(d+c)^2 ca} \right. \\
&- \frac{3\varphi^2 a}{32(d+c)^2 d} - \frac{3\varphi^4}{64(d+c)^2 cb} - \frac{3\varphi^2 b}{16(d+c)^2 c} + \frac{7}{8} + \frac{5c}{32d} \\
&+ \left. \frac{3d}{32c} \right) T^2 \lambda^2 \pi^{-2}. \tag{B.3}
\end{aligned}$$

Similarly, it is easy to get the corresponding Higgs mass-squared of order g^4 , λ^2 and f_t^4 .

$$\begin{aligned}
m_\varphi^{(3)^2} = & g^2 c^2 + \left(-\frac{27 \varphi^4}{512 c^3 a} + 3/4 - \frac{9 \varphi^2 b}{64 d^3} - \frac{9 \varphi^2 a}{128 d^3} \right. \\
& - \frac{27 \varphi^2 a}{128 c^3} - \frac{27 \varphi^2 b}{64 c^3} + \frac{9 d}{32 c} + \frac{3 c}{32 d} - \frac{27 \varphi^4}{256 c^3 b} \Big) T^2 \lambda^2 \pi^{-2} \\
& + \left(\frac{9 \varphi^2}{256 c b} + \frac{9 a}{128 c} + \frac{9 b}{64 d} + \frac{9 b}{64 c} + \frac{9 \varphi^2}{512 c a} + \frac{9 a}{128 d} \right) \lambda T^2 g^2 \pi^{-2} \\
& + \left(-\frac{9 \varphi^2}{4 c} - \frac{3 \varphi^2}{4 d} \right) \lambda^2 T \pi^{-1} g^{-1} \\
& + \left(-\frac{3 \varphi^2 c}{32 d^3} - \frac{27 \varphi^2 d}{32 c^3} + \frac{3 \varphi^2}{8 d (d + c)} + \frac{9 \varphi^2}{32 c d} - \frac{15 \varphi^2}{32 d^2} \right) \lambda^3 T^2 \pi^{-2} g^{-2} \\
& + \left(-\frac{c^2}{256 b (d + c)} + \frac{3 b}{32 a} - \frac{d^2}{256 b (d + c)} + \frac{c d}{128 b (d + c)} \right. \\
& + \frac{\varphi^2}{128 b (c + b)} + \frac{9 d}{512 a} - \frac{3 \varphi^2 b}{128 a^3} - \frac{3 \varphi^4}{2048 a^3 (c + a)} - \frac{9 \varphi^2 d}{2048 a^3} \\
& - \frac{3 \varphi^2 c}{2048 a^3} + \frac{\varphi^2 d^2}{1024 b^3 (d + c)} - \frac{\varphi^4}{512 b^3 (c + b)} - \frac{\varphi^2 d c}{512 b^3 (d + c)} \\
& + \frac{3 \varphi^2}{512 a (c + a)} + \frac{\varphi^2 c^2}{1024 b^3 (d + c)} + \frac{3 c}{512 a} \Big) T^2 g^4 \pi^{-2} \\
& + \left(-\frac{3 \varphi^2}{64 a} - \frac{3 \varphi^2}{32 b} - \frac{3 b}{8} - \frac{3 a}{16} \right) T g^3 \pi^{-1} \\
& + \left(-\frac{81 \varphi^4}{32 c^4} - \frac{3 \varphi^4}{8 d^3 (d + c)} - \frac{27 \varphi^4}{32 c^3 d} \right) \lambda^4 T^2 \pi^{-2} g^{-4} \\
& + \frac{\left(-\frac{3 c}{4} - \frac{3 d}{4} \right) \lambda T g}{\pi}. \tag{B.4}
\end{aligned}$$

According to (49) the masses determine the effective potential of order g^4 , λ^2 and f_t^4

$$V^{(3)}(\varphi, T) = \int^\varphi d\varphi' m_\chi^{(3)^2}(\varphi', T). \tag{B.5}$$

Due to the complicated structure in φ of the integral, (a, c and d are irrational functions of φ) we have not evaluated it analytically. Instead of it, we have

used a numerical integration in order to determine the effective potential at the critical temperature and to calculate the surface tension.

Appendix C Coset space volume

Due to the global $SU(2) \times U(1)$ symmetry of the standard model, which is spontaneously broken to the electromagnetic $U(1)$ subgroup, the fluctuations around the saddle point (cf. eq. (79)) contain three zero modes which have to be treated in the usual way by the method of collective coordinates.

An infinitesimal transformation of the saddle point $\bar{\Phi}$, which yields another saddle point with the same free energy, is given by

$$d\Phi = dU\bar{\Phi} = i \sum_{i=1}^3 d\omega_i T_i \bar{\Phi} \quad , \quad (C.1)$$

where

$$T_{1,2} = \frac{1}{2}\tau_{1,2}, \quad T_3 = \frac{1}{2}(\tau_3 - E) \quad ; \quad (C.2)$$

here E denotes the identity matrix. Transformations generated by $T_4 = \frac{1}{2}(\tau_3 + E)$ leave the saddle point $\bar{\Phi}$ invariant. Comparing eq. (C.1) with

$$d\Phi = \frac{1}{\sqrt{2}} \begin{pmatrix} d\chi_1 + id\chi_2 \\ id\chi_3 \end{pmatrix}, \quad (C.3)$$

yields the connection between the fields $d\chi_i$ and the group parameters $d\omega_i$. The corresponding measure of the functional integral is

$$[d\chi] = \prod_{i=1}^3 \left(\frac{\beta}{2\pi} \right)^{\frac{1}{2}} dc_i, \quad (C.4)$$

where $d\chi_i = \xi_i dc_i$, and ξ_i is a normalized function, i.e., $\int d^3x \xi_i^2 = 1$. Eqs. (C.1), (C.3) and (C.4) yield

$$[d\chi] = -\frac{1}{4} \left(\frac{\beta}{2\pi} \int d^3x \bar{\varphi}^2 \right)^{\frac{3}{2}} \prod_{i=1}^3 d\omega_i. \quad (C.5)$$

From eqs. (C.1) and (C.2) one can easily calculate the metric on the group manifold at the origin $\omega = 0$:

$$g_{ij} = -tr(U^{-1} \frac{\partial}{\partial \omega_i} U U^{-1} \frac{\partial}{\partial \omega_j} U) = c(i) \delta_{ij}, \quad (C.6)$$

where

$$c(1) = c(2) = \frac{1}{2}, \quad c(3) = c(4) = 1, \quad (\text{C.7})$$

$$\sqrt{\det g(\omega = 0)} = \frac{1}{2}. \quad (\text{C.8})$$

Globally, the symmetry group acting on the Higgs field is not $SU(2) \times U(1)$, but rather $SO(3) \times Z_2 \times SO(2)$, where the elements of Z_2 are E and $-E$, and $SO(2)$ corresponds to phase transformations with the phase varying from 0 to π . For the normalization (C.8) the volume of this group is (cf. ref. [31])

$$\int d\omega_1 \dots d\omega_4 \sqrt{g} = 2\pi^3. \quad (\text{C.9})$$

The Higgs vacuum expectation value breaks this symmetry to the subgroup $U(1)$. The corresponding volume of the coset space is

$$V(SO(3) \times Z_2 \times SO(2)/U(1)) = \pi^2. \quad (\text{C.10})$$

For the integration over the zero modes one now obtains

$$\int [d\chi] = \frac{\pi^2}{2} \left(\frac{\beta}{2\pi} \int d^3x \bar{\varphi}^2 \right)^{\frac{3}{2}}. \quad (\text{C.11})$$

The corresponding three eigenvalues in the symmetric phase are $\sim \mu^2$, where $\mu = m_\varphi(0, T)$. Hence, the relative contribution of the zero modes to the nucleation rate Γ is $\mu^3 \int [d\chi]$.

References

- [1] D. A. Kirzhnits and A. D. Linde, Phys. Lett. B72 (1972) 471.
- [2] S. Weinberg, Phys. Rev. D9 (1974) 3357;
L. Dolan and R. Jackiw, Phys. Rev. D9 (1974) 3320;
D. A. Kirzhnits and A. D. Linde, Ann. Phys. 101 (1976) 195.
- [3] V. A. Kuzmin, V. A. Rubakov and M. E. Shaposhnikov, Phys. Lett. B155 (1985) 36.
- [4] K. Enqvist et. al., Phys. Rev. D45 (1992) 3415.
- [5] M. Dine et al., Phys. Rev. D46 (1992) 550.
- [6] M. E. Carrington, Phys. Rev. D45 (1992) 2933.
- [7] C. G. Boyd, D. E. Brahm and S. D. H. Hsu, preprint CALT-68-1795 (1992);
M. E. Shaposhnikov, Phys. Lett. B277 (1992) 324; Erratum-ibid. B282 (1992) 483.
- [8] W. Buchmüller, T. Helbig and D. Walliser, preprint DESY-92-151.
- [9] J.R. Espinosa, M. Quirós and F. Zwirner, preprint CERN-TH.6577/92, IEM-FT-58/92.
- [10] P. Arnold, Phys. Rev. D46 (1992) 2628;
P. Arnold and O. Espinosa, preprint UW/PT-92-18 (1992).
- [11] R. R. Parwani, Phys. Rev. D45 (1992) 4695.
- [12] V. Jain, preprint MPI-Ph/92-72 (1992);
V. Jain and A. Papadopoulos, preprint LBL-33067 (1992) ;
M. Carena and C. E. M. Wagner, preprint MPI-Ph/92-67 (1992).
- [13] N. Tetradis and C. Wetterich, preprint DESY 92-117 (1992);
M. Reuter and C. Wetterich, preprint HD-THEP-92-62 (1992).
- [14] H. Meyer-Ortmanns and A. Patkós, Phys. Lett. B297 (1992) 321.

- [15] D. O'Connor, C. R. Stephens and F. Freire, preprint DIAS-STP-92-02 (1992).
- [16] B. Bunk et al., Phys. Lett. B284 (1992) 371.
- [17] M. Gleiser, E. W. Kolb and R. Watkins, Nucl. Phys. B364 (1991) 411;
N. Tetradis, preprint DESY 91-151, Z. Phys. C, in press;
M. Gleiser and E. W. Kolb, Phys. Rev. Lett. 69 (1992) 1304,
and preprint FERMILAB-Pub-92/222-A;
M. Gleiser and R. O. Ramos, Phys. Lett. B300 (1993) 271.
- [18] J. Langer, Ann. Phys. 41 (1967) 108; *ibid.* 54 (1969) 258.
- [19] J. I. Kapusta, Finite Temperature Field Theory, (Cambridge University Press, Cambridge, 1989).
- [20] E. J. Weinberg and A. Wu, Phys. Rev. D36 (1987) 2474.
- [21] B. A. Freedman and L. D. McLerran, Phys. Rev. D16 (1977) 1130.
- [22] A. D. Linde, Phys. Lett. 96B (1980) 289;
D. J. Gross, R. D. Pisarski and L. G. Yaffe, Rev. Mod. Phys. 53 (1981) 43.
- [23] A. Billoire, G. Lazarides and Q. Shafi, Phys. Lett. B103 (1981);
J. E. Mandula and M. Ogilvie, Phys. Lett. B201 (1988) 117;
O. K. Kalashnikov, Phys. Lett. B279, (1992) 367.
- [24] A. D. Linde, Nucl. Phys. B216 (1983) 421.
- [25] C. Callan and S. Coleman, Phys. Rev. D16 (1977) 1762.
- [26] N. J. Günther, D. A. Nicole and D. J. Wallace, J. Phys A: Math. Gen. 13 (1980) 1755.
- [27] W. Buchmüller and T. Helbig, Int. J. Mod. Phys. C3 (1992) 799.
- [28] L. P. Csernai and J. I. Kapusta, Phys. Rev. D46 (1992) 1379;
M. E. Carrington and J. I. Kapusta, preprint TPI-MINN-92/55-T(1992).
- [29] D. Bödeker, W. Buchmüller, Z. Fodor and T. Helbig, in preparation.

- [30] E. Braaten and R. Pisarski, Nucl. Phys. B337 (1990) 569.
- [31] M. Lüscher, unpublished notes;
R. Gilmore, Lie Groups, Lie Algebras, and Some of Their Applications
(Wiley & Sons, New York, 1974).

Figure caption

Figure 1 : One-loop contributions to the effective potential.

Figure 2 : Two-loop contributions to the effective potential.

Figure 3 : Ring diagram contributions to the effective potential with one-loop self-energy insertions.

Figure 4 : One-loop self-energy contributions to the gauge-boson.

Figure 5: One-loop contributions to the effective potential with full propagators including counterterms.

Figure 6: The gap equations: All one-loop self-energy corrections with full propagators.

Figure 7: The maximal value of the Higgs mass for which the phase transition is first-order as function of γ .

Figure 8: The maximal Higgs mass as function of the convergence parameter ξ . (The dependence on the top-quark mass is smaller than the width of the line.)

Figure 9: The effective potential to order g^3 and $\lambda^{3/2}$ at the smallest temperature (T^*) allowed for $\xi = 2$.

Figure 10: Surface tension as function of the Higgs mass for different values of γ .

Figure 11: Surface tension as function of the Higgs mass with the $\lambda^{3/2}$ -contributions (full line), with λ -contributions only (long-dashed line) and with contributions from the partial summation of g^4 and λ^2 terms (short-dashed line).

Figure 12: The potentials $U_\varphi(r)$ and $U_\chi(r)$ for the scalar fluctuations $\hat{\varphi}$ and $\hat{\chi}$.

Figure 13: The potential \bar{V} for three different Higgs masses at the corresponding nucleation temperatures T_e . The potential for $m_H = 100 \text{ GeV}$ (200 GeV) has been multiplied reduced by a factor 10 (factor 400).

